BMC Structural Biology

Research article

Open Access

Characterization of a human coagulation factor Xa-binding site on *Viperidae* snake venom phospholipases A_2 by affinity binding studies and molecular bioinformatics

Grazyna Faure*[1], Veerabasappa T Gowda[2] and Rachid C Maroun*[3]

Address: [1]Unité d'Immunologie Structurale, Institut Pasteur, 25 rue du Dr. Roux, 75724 Paris Cedex 15, France, [2]University of Mysore, Department of Studies in Biochemistry, Manasagangothri, 570006 Mysore, India and [3]INSERM, Centre Paul Broca, 2-ter rue d'Alésia, 75014 Paris, France

Email: Grazyna Faure* - fgrazyna@pasteur.fr; Veerabasappa T Gowda - tvguom@hotmail.com; Rachid C Maroun* - rmaroun@gmail.com

* Corresponding authors

Published: 6 December 2007

BMC Structural Biology 2007, **7**:82 doi:10.1186/1472-6807-7-82

Received: 13 April 2007

Accepted: 6 December 2007

This article is available from: http://www.biomedcentral.com/1472-6807/7/82

Abstract

Background: The snake venom group IIA secreted phospholipases A_2 ($SVPLA_2$), present in the *Viperidae* snake family exhibit a wide range of toxic and pharmacological effects. They exert their different functions by catalyzing the hydrolysis of phospholipids (PL) at the membrane/water interface and by highly specific direct binding to: (i) presynaptic membrane-bound or intracellular receptors; (ii) natural PLA_2-inhibitors from snake serum; and (iii) coagulation factors present in human blood.

Results: Using surface plasmon resonance (SPR) protein-protein interaction measurements and an *in vitro* biological test of inhibition of prothrombinase activity, we identify a number of *Viperidae* venom $SVPLA_2$s that inhibit blood coagulation through direct binding to human blood coagulation factor Xa (FXa) via a non-catalytic, PL-independent mechanism. We classify the $SVPLA_2$s in four groups, depending on the strength of their binding.

Molecular electrostatic potentials calculated at the surface of 3D homology-modeling models show a correlation with inhibition of prothrombinase activity. In addition, molecular docking simulations between $SVPLA_2$ and FXa guided by the experimental data identify the potential FXa binding site on the $SVPLA_2$s. This site is composed of the following regions: helices A and B, the Ca^{2+} loop, the helix C-β-wing loop, and the C-terminal fragment. Some of the $SVPLA_2$ binding site residues belong also to the interfacial binding site (IBS). The interface in FXa involves both, the light and heavy chains.

Conclusion: We have experimentally identified several strong FXa-binding $SVPLA_2$s that disrupt the function of the coagulation cascade by interacting with FXa by the non-catalytic PL-independent mechanism. By theoretical methods we mapped the interaction sites on both, the $SVPLA_2$s and FXa. Our findings may lead to the design of novel, non-competitive FXa inhibitors.

Background

Haemostasis (vasoconstriction, platelet plug formation and blood clotting) is a defense mechanism that evolved to prevent the loss of blood after injury to the transporting vessels [1]. The intrinsic and the extrinsic alternate pathways initiate the blood clotting process. One of the com-

mon steps in both pathways of coagulation is the activation of coagulation factor X (FX) to factor Xa (FXa).

FXa circulates in plasma as the light and the heavy chains connected by a single disulfide linkage. The N-terminal region of the light chain (residues 1–39) is the Gla domain, rich in post-translationaly modified γ-carboxyglutamic acid, which interacts with the phospholipid (PL) membrane[2]. The Gla domain is followed by a short stack of hydrophobic residues (residues 40–45), and two epidermal growth factor-like repeats – the EGF-like 1 domain (residues 46–84) and the EGF-like 2 domain (residues 85–128). The heavy chain of FXa contains the catalytically active serine proteinase domain (254 amino acids, residues 16–269 in chymotrypsinogen numbering system). As a serine proteinase of the chymotrypsin family [3], FXa consists of two subdomains of antiparallel β-barrel structure each comprising a sheet of six strands and four helices. Residues His57, Asp102, and Ser195 (chymotrypsinogen numbering) form a catalytic triad at the active site cleft between the two subdomains[4]. The fold contains a number of solvent-exposed loops, which determine S1 and subsite preferences in structurally homologous enzymes of the family. To the north of the active site cleft in the canonical view are the 60- and 99-loops; to the west are the 174 – and the 217–225 loops, restricting access to the active site. The autolysis loop 149–151 occupies the southern boundary of the active site cleft. Adjacent to it is the 70-loop. To the east is the 37-loop. Loop 185–188 is associated with S1 preference[5,6]. Upon binding to FVa in the presence of Ca^{2+} ions on negatively charged membrane PL at the cellular surface, the prothrombinase complex is formed, resulting in the accelerated conversion of FII (prothrombin) to FIIa (thrombin) by FXa [7,8]. Afterwards, thrombin converts fibrinogen into fibrin, consolidating the primary plug.

Secreted phospholipases A_2 ($sPLA_2$, EC 3. 1. 1. 4) are water-soluble interfacial enzymes that catalyze the hydrolysis of the 2-acyl groups in 3-*sn*-phosphoglycerides. The His48/Asp99 pair, the 26–34 calcium-binding loop and the 69-loop of residues 59–74 constitute the catalytic site. The calcium metal is a cofactor and its pocket is composed of Asp49 and the calcium-binding loop [9]. The Interfacial Binding Site (IBS) of several PLA_2s has been located and is species- and enzyme class-specific [10-12]. In human non-pancreatic secreted group IIA phospholipase A_2 ($hsPLA_2$), the IBS is located in the "front" face of the enzyme [13,14]. It consists of a highly hydrophobic surface (Val3, Ala18, Leu19, Phe24, Phe70 and Tyr119) that surrounds the active site, and of hydrophilic residues (Arg7, Lys10, Glu16, and His6) (PDB code 1BBC; numbering system throughout as in Renetseder *et al.* [15]). Two other residues (Lys74 and Lys115) lie in the periphery of the IBS[13].

In addition to the esterase activities, $sPLA_2$s are also specific ligands that interact with different targets, such as membrane-bound PLA_2 receptors [16,17], anionic heparan sulfate proteoglycans (HSPG)[18,19], and with a cytoskeleton protein (vimentin)[20]. On the other hand, the soluble receptors of PLA_2s, such as the natural inhibitors in the blood of snakes, the coagulation factors, and the PLA_2 binding protein have been also well characterized[21,22]. Hence, it has become clear that PLA_2s exert physiological and patho-physiological effects through protein-protein interaction and/or protein-PL interactions[22,23]. These protein-protein mechanisms are sometimes dependent on, and other times independent of their enzymatic activity, playing important roles in determining the specific function of $sPLA_2$s [24-26]. *Viperidae* snake venoms contain several toxic group IIA PLA_2s ($SVPLA_2$), which may act as presynaptic neurotoxins[27] and may interfere with blood coagulation by possessing strong anticoagulant properties [28-40]. *Viperidae* $SVPLA_2$s have high primary sequence identity with human group IIA PLA_2 ($hsPLA_2$; 30–60%) and overall structural homology[41,42]. Almost all anticoagulant snake venom PLA_2 are basic proteins and may inhibit coagulation by several mechanisms. A first mechanism involves the hydrolysis and destruction of procoagulant PL [43-47]. CM-I and CM-II, illustrate this mechanism in which the group I PLA_2 inhibits the extrinsic tenase complex [22,43], and does not bind to FXa. A second mechanism is based on the competition with clotting proteins for binding to the lipid surface due to the high affinity of PLA_2 toward PL the "antagonist effect" [28,48][49]. A third mechanism is a non-enzymatic, PL-independent mechanism in which the PLA_2 interacts with FXa, inhibits the prothrombinase complex by preventing formation of the FXa/FVa complex and introduces a lag time in the generation of thrombin[22,32,34,35,39,50,51]. In addition, some snake venom PLA_2s show a combination of enzymatic and non-enzymatic mechanisms, like the basic $sPLA_2$ isoform CM-IV from *Naja nigricollis (Elapidae)* venom[22,29].

The non-enzymatic inhibition mechanism of the prothrombinase complex was first demonstrated for CM-IV[32,34] and then for $hsPLA_2$ [50]. The catalytically inactive His48Gln mutant of $hsPLA_2$ possesses an identical anticoagulant effect and binds to FXa with the same kinetic constant as the wild-type enzyme, showing that in this mechanism the anticoagulant process is independent of the catalytic activity of the PLA_2 [51].

Kini and Evans first proposed that a "pharmacological site," in addition to the catalytic site, could explain the specific biological anticoagulant activity of snake venom group I PLA_2s[33]. This anticoagulant region consists of the basic exposed loop located in the region 55–70, and

the beginning of the β-sheet on *Elapidae* group I PLA_2s [52,53]. The proposed region is positively charged in strong anticoagulant enzymes, but negatively charged in weak and non-anticoagulant enzymes [33]. More recently, Kini proposed that weakly anticoagulant enzymes, which lack the anticoagulant region, fail to bind specifically to FXa in the coagulation cascade [22].

In spite of all the studies, the corresponding site in *Viperidae* $SVPLA_2$s is not yet clearly established. In addition, no distinction is usually made between the mechanisms by which the anticoagulant potency is exerted by the PLA_2s. It seems that only the mechanisms that imply participation of PL have been taken into account in the past.

Anticoagulant snake venom PLA_2 represent a novel family of agents useful in identifying the sites of interaction of anticoagulants at the level of specific amino acid residues and thus have a potential in identifying new drug leads [54]. In order to characterize the FXa-binding site of $SVPLA_2$ from the *Viperidae* family, we have focused on the non-enzymatic, PL-independent, anticoagulant mode of action. Previous work from the Unité des Venins (Institut Pasteur, Paris) had shown the involvement of basic residues located around the IBS of $hsPLA_2$ [51], on one hand, and the possible involvement of the C-terminal and β-wing regions of AtxA[39] in binding to FXa, on the other. We were henceforth interested in determining whether similar or different amino acid patterns were present in *Viperidae* $SVPLA_2$s. Using SPR and a physiological test of inhibition of prothrombinase activity, we identified $SVPLA_2$s that formed complexes with FXa and determined the apparent affinity constants of the complexes. With this experimental information at hand, we applied sequence analysis, molecular bioinformatics and docking procedures in order to define the anticoagulant region of the PLA_2 and the nature of the residues involved in the interaction with FXa.

The $SVPLA_2$s tested in this study are: CBc and CBa_2, two isoforms of the basic subunit of crotoxin (CTX), a non covalent, heterodimeric toxin from *Crotalus durissus terrificus* formed by the basic CB and the acidic CA subunits [55]; CA_2, an isoform of the acidic subunit of CTX[56]; the acidic and basic subunits of the β-neurotoxin from *Pseudocerastes fieldi*[57] (CbI and CbII); isoform A of ammodytoxin from *Vipera ammodytes ammodytes*[58] (AtxA); the PLA_2 from *Vipera berus berus*[59] (*Vbb*); Myotoxin II (inactive Asp49Lys mutant) [60] from *Bothrops asper*[61] (MtxII); PLA_2 from *Daboia russelli pulchella* [62] (VRV-PLVIII); the basic PLA_2 from *Agkistrodon halys pallas* [63] (*bAhp*); agkistrodotoxin from *Agkistrodon halys pallas*[64] (AGTX); PLA_2 from *Crotalus atrox* [65] (*Catx*). We also tested human group IIA PLA_2[66] ($hsPLA_2$; Uniprot P14555; PDB 1BBC). The crystal structures of MtxII, VRV-PLVIII, *bAhp*, AGTX, *Catx* and $hsPLA_2$ are available in the PDB, whereas we structure-modeled CBc, CBa_2, CbI, CbII, AtxA and *Vbb*.

Results

Identification of $SVPLA_2$s that bind to FXa and inhibit prothrombinase activity

As shown in Table 1, the $SVPLA_2$s from *Viperidae* snake CBc and MtxII interact with FXa with very high affinity

Table 1: FXa binding kinetic parameters and effect on prothrombinase activity of *Viperidae* $SVPLA_2$

PLA_2	$<k_{on}>(M^{-1}s^{-1})$	$<k_{off}>$ (s^{-1})	$<K_d^{app}>$[nM]	IC_{50}[nM]	pI*
CBc	$(3.2 \pm 0.2) \times 10^5$	$(1.6 \pm 0.4) \times 10^{-4}$	0.6 ± 0.3	0.7 ± 0.3	8.74
MtxII	$(10.4 \pm 0.3) \times 10^6$	$(1.78 \pm 0.4) \times 10^{-2}$	1.8 ± 0.9	3 ± 1	9.10
CbII	$(4.2 \pm 2.5) \times 10^5$	$(8.5 \pm 2) \times 10^{-3}$	20 ± 3	20 ± 4	8.96
AtxA	$(2.2 \pm 0.3) \times 10^5$	$(7 \pm 1) \times 10^{-3}$	30 ± 2	25 ± 5	8.35
CBa_2	$(2.9 \pm 0.4) \times 10^5$	$(1.5 \pm 0.2) \times 10^{-2}$	52 ± 4	41 ± 5	8.74
VRV-PLVIII	$(4.5 \pm 0.4) \times 10^4$	$(2.6 \pm 0.4) \times 10^{-2}$	578 ± 15	130 ± 20	8.35
bAhp	$(4 \pm 1.5) \times 10^4$	$(1.6 \pm 0.3) \times 10^{-2}$	400 ± 20	90 ± 10	8.71
Vbb	$(3 \pm 0.5) \times 10^4$	$(2.5 \pm 0.4) \times 10^{-2}$	830 ± 15	90 ± 30	8.64
AGTX	NB	NB	NB	>10 000	5.43
CA	NB	NB	NB	>10 000	-
Catx	NB	NB	NB	>10 000	4.64
CbI	NB	NB	NB	>10 000	4.86
Reduced and carboxymethylated CBc	NB	NB	NB	nd	nd
$hsPLA_2$	$(2.0 \pm 0.8) \times 10^6$	$(2.9 \pm 1) \times 10^{-2}$	14 ± 2	9 ± 2	9.38

*: estimated
NB: non-binding
Nd: not determined
$<K_d^{app}>$ = <koff>/<kon>
The IC_{50} value corresponds to 50% inhibition of thrombin generation in the absence of PL for the different $SVPLA_2$.

and constitute group VS (<K_d^{app}> 0.6 – 2 nM). These enzymes strongly inhibit the formation of the prothrombinase complex (IC_{50} 1–3 nM). Under identical conditions, the <K_d ^{app}> value determined for hsPLA_2 is 14 nM. CBa_2, AtxA and CbII have high affinity values and anticoagulant potency, and form group S (20–50 nM). A third group of $SVPLA_2$, group M, is formed by *Vbb*, VRV-PLVIII, and *bAhp*. In this group, the affinity with FXa is smaller (<K_d^{app}> 400 – 830 nM) and the IC_{50} ranges from 90 to 130 nM. AGTX (the neutral PLA_2 from *A. halys pallas (blomhoffii)*), reported previously as weakly anticoagulant in the presence of PL[38], does not interact with FXa and does not inhibit prothrombinase activity in the absence of PL. Neither CbI nor *Catx* inhibit prothrombinase activity in the absence of PL. These three $SVPLA_2$s constitute group NB. Last, reduced and carboxymethylated CBc does not interact with FXa. Furthermore, we found a positive linear correlation between <K_d ^{app}> and IC_{50} (R = 0.995) for the three groups of $SVPLA_2$ that interact with FXa. Thus, the strongly anticoagulant $SVPLA_2$s bind with high affinity to FXa, whereas the less efficient anticoagulant $SVPLA_2$ possess low affinity for FXa. Also, basic $SVPLA_2$s (8.35<pI<9.10) bound to FXa and inhibited prothrombinase activity, whereas those with acidic pIs (4.60–5.43) did not (Table 1).

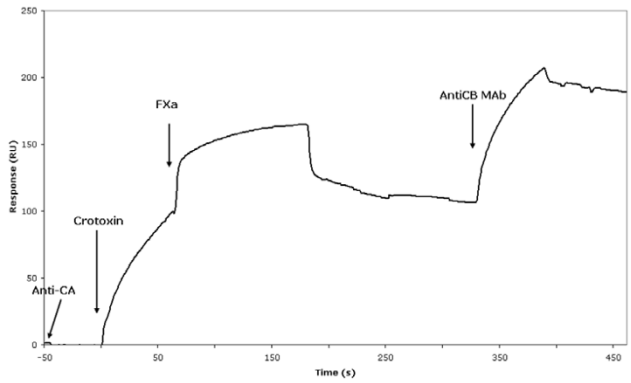

Figure 1
The interaction between an isoform of CTX and FXa, as measured by SPR. The anti-CA monoclonal antibody mAb A-73.13 [70] was covalently attached to the chip [71]. CTX (the CA_2-CBc complex) was then captured via this mAb before injection of FXa (25 μg/ml). FXa bound to CTX, as seen in the rise of the resonance signal, showing that the CTX-FXa complex remained attached to the anti-CA mAb. After injection of a specific anti-CB MAb (B-32.13, 10 μg/ml), the signal increased further, confirming the presence of CB in the ternary CA-CB-FXa complex.

It is interesting to note that the isoenzymes CBc and CBa_2, which differ by 8 amino acids (His1Ser, Ile18Val, Arg34Gln, Pro74Arg, Glu92Lys, Tyr115Asn, Gly116Glu, Gly128Glu) and associate with the acidic subunit CA to form two pharmacologically distinct classes of crotoxin complexes, present differences in toxicity, enzymatic activities and stability[67,68]. These two isoforms bind to FXa with different kinetics (Table 1). The average rate of dissociation constant <k_{off}> for the FXa-CBa_2 complex is about two orders of magnitude greater than that of the FXa-CBc complex, implying a more stable FXa-CBc complex (<K_d ^{app}> 0.6 nM). Consequently, CBc strongly inhibits the prothrombinase complex (IC_{50} 0.7 nM), whereas the inhibition by CBa_2 is much weaker (IC_{50} 41 nM). Indeed, we had observed in the past that the difference in stability between crotoxin isoforms was due only to the CB subunit [55,68].

We also investigated by SPR the possibility of the formation of a ternary CA-CB-FXa complex. On one hand, CA binds to immobilized CB [69], whereas FXa does not interact with immobilized CB[23]. An anti-CA monoclonal antibody (mAb) A-73.13 [70] was covalently attached to the chip, as previously described [71]; CTX was then captured via this mAb before the injection of FXa (Fig. 1). FXa bound to CTX, as seen in the rise of the resonance signal. Fig. 1 also shows that after the injection of a specific anti-CB mAb (B32.13), the signal increased further, indicating the presence of CB on the chip and showing that the CB-FXa complex is stable and remained attached to CA.

Sequence analysis, comparisons and consensus residues of the anticoagulant $SVPLA_2$s

In order to identify those residues or sequence patterns that differ between members of the $SVPLA_2$s, we obtained Weblogo plots of the four groups VS (CBc, MtxII), S (CbII, AtxA, CBa_2), M (VRV-PLVIII, *bAhp*, *Vbb*) and NB (AGTX, *Catx*, CbI). Thereafter, we performed comparisons of all the sequences among themselves and of the four groups against each other.

Considering only segments of three or more residues, we observed three conserved regions for AGTX, *Catx* and CbI of the NB group (Tyr25-Gly30, Thr41-Gly53 and Cys96-Asp99; Fig. 2A), and six for the CBc-MtxII pair of the VS group (Tyr25-Cys27, Gly33-Gly35, Pro37-Cys45, Cys50-Tyr52, Cys96-Asp99 and Cys105-Arg107; Fig. 2B). A striking difference between the two groups is the presence of the acidic residue Glu at position 128 in the C-terminal region of all $SVPLA_2$s of the NB group, as opposed to a Lys or a Gly residue in the VS group. For the other groups, only CBa_2 and *Vbb* contain a Glu at this position. With respect to the S group, the M group contains a conserved basic residue at position 115. Interestingly, the M group contains a conserved Lys in position 132 that is absent in the VS and NB groups. Group NB contains acidic side chains in the first strand of the β-wing and the adjacent β-

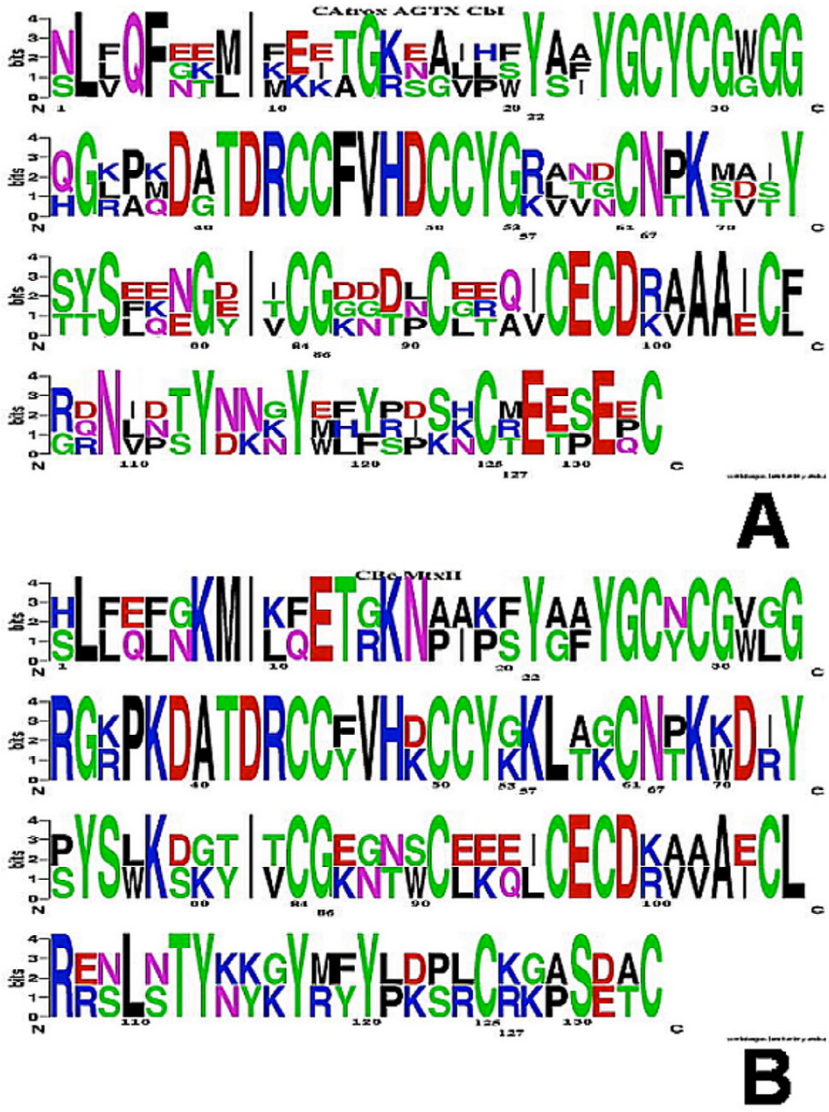

Figure 2
Weblogo representation of the multiple sequence alignment of the SVPLA$_2$s. A. Group NB (AGTX, *Catx* and CbI). Each logo consists of stacks of symbols, one stack for each position in the sequence. The overall height of the stack indicates the sequence conservation at that position, while the height of symbols within the stack indicates the relative frequency of each amino acid at that position. The symbols in each stack are arranged by alphabetical order from top to bottom and do not follow the order in which the sequences were fed. Arg, His and Lys residues are in blue; Asp and Glu in red; Ala, Ile, Leu, Met, Phe, Pro, Trp, and Val in black; Gly, Cys, Ser, Thr, and Tyr in green; Asn, Gln in purple. Renetseder numbering system for all PLA$_2$s throughout this work [15]. B. Group VS (CBc and MtxII).

turn (residues 75–82). For the VS and S groups, the tendency is towards a net balance of positive charges in the β-wing.

The NB group *Catx* presents three Glu and one Asp residue in the β-wing (residues 74–90); CbI presents two Asp residues. The β-wing of CBc of group VS contains two Lys residues; that of MtxII two Lys, one Asp and one Glu residues. For the S and M groups the tendency is towards net positive charges, except for *bAhp*, for which the total charge is neutral.

Tertiary structures and molecular electrostatic potentials of SVPLA$_2$s

We obtained 3D homology models of CBc, CBa$_2$, CbI, CbII, AtxA and *Vbb*. The models show the canonical struc-

tural features of the PLA_2 template molecules: a N-terminal α-helix (helix A), a short helix (helix B), a Ca^{2+}-binding loop, a long α-helix (C), a loop preceding an anti-parallel two-stranded sheet (β-wing), a long α-helix (D), anti-parallel to helix C, and a C-terminal extended fragment. All seven disulfide-bridges are at their expected positions. Fig. 3 shows the molecular model of AtxA in the canonical ("front") face orientation, i.e., presenting the catalytic hydrophobic channel.

Fig. 4A shows the MEP calculated at the molecular surface of the modeled $SVPLA_2$s in the canonical view. Fig. 4B shows the MEP on the "back" face. Qualitatively, we observe that the MEP is positive in the front face of strong and mild anticoagulants (CBc, CBa_2, CbII, and AtxA); approximately neutral for the weak anticoagulant *Vbb*, and negative for CbI (Fig. 4A). The back face is largely devoid of positive potential, except for *Vbb* (Fig. 4B). This difference in MEP leads to an electrostatic asymmetry. We observe the same trend for the crystallized $SVPLA_2$ (MtxII, VRV-PLVIII, *bAhp*, AGTX, *Catx* and $hsPLA_2$; not shown).

Molecular docking and intermolecular interfaces: mapping of the anticoagulant site and of the binding site on FXa

The output generated by the docking program PatchDock showed many complexes in contact with one of the binding site regions. Only the AtxA-FXa candidate complex (rank number 7) showed the best compatibility with the binding site derived from the mutagenesis data[39] (in this complex, position 150, which shows a Glu -> Arg sequence difference between the purchased FXa and the crystal structure (PDB entry 2BOH) is neither at the light/heavy chains interface nor at the AtxA/FXa interface). Several residues belonging to the two regions identified by the mutagenesis of AtxA and defining part of the binding site (the "front" strand of the β-wing and the C-terminal fragment) are at the interface in this complex. In it, the relative orientation of FXa positions the N-terminus of the EGF-like 2 domain of the light chain of FXa towards the β-wing of AtxA, allowing the 1-domain (not visible in the X-ray structure) to enter in interaction with the β-wing and thus contact the remaining residues of the front edge of the β-wing. Fig. 5 shows the ribbon representation of the final complex between AtxA and the light and heavy chains of FXa. Fig. 6 shows the same complex in the form of a solvent-accessible surface. In both representations, the $SVPLA_2$ is in the "classical" orientation, i.e. that of Fig. 4A. Overall, we observe just small conformational changes after complex formation.

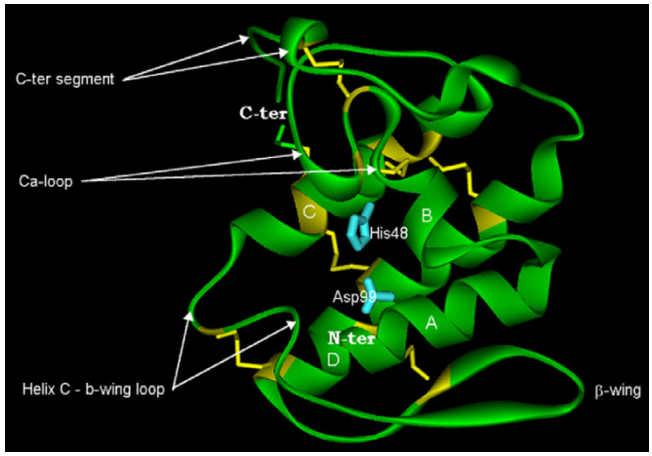

Figure 3
Ribbon diagram of the molecular model of AtxA. α-helices A, B, C and D, and the β-wing are labeled. The seven-disulfide bridges are in yellow sticks and the His48/Asp99 pair in cyan sticks.

For the FXa strong-binding $SVPLA_2$s CBc, MtxII, CbII and CBa_2, the complexes that ranked 18, 10, 20 and 17, respectively, showed the same binding mode as the AtxA-FXa complex, i.e., the same relative orientation of FXa with respect to the $SVPLA_2$. As measured by the FIT function of Pymol, these complexes showed Cα RMSD's with respect to the reference AtxA-FXa complex of 3.4, 2.2, 5.1 and 4.8 Å, respectively.

The percentage of surface residues at the interface of the complexes is of 24–36% for the five $SVPLA_2$s and of 20–32% for FXa. The interface area for the five $SVPLA_2$s is in the 860–1700 $Å^2$ range and 915–1470 $Å^2$ for FXa. The interface area of the complexes varies from 1610 to 1930 $Å^2$. The values obtained for the solvent accessible area buried in the five characterized complexes fall between the small and the large interfaces categories in a study of 362 protein-protein interfaces [72]. Fig. 7 shows the mapping of the $SVPLA_2$-FXa interaction surface of the complexes between the five $SVPLA_2$s and FXa. The shadowed residues in that figure are those at the interface of the AtxA-FXa complex satisfying the mutagenesis data, and at the interface of the complexes of the other four $SVPLA_2$s that show the same complexation mode as the AtxA-FXa complex. The consensus residues that participate to FXa binding are: solvent-exposed parts of helix A (positions 2, 3, 7) and helix B (positions 18, 19); positions 16, 23 and 24; a part of the Ca^{2+} loop (positions 31–34); a part of the 69-loop (between helix C and the β-wing; positions 53, 59, 60, 69 and 70); and the C-terminal segment (positions 118, 119, 121–124, 129–131, 133). By taking into account the type of atom-atom contacts as defined by Sobolev *et al.*[73], 36.5% of the contacts are hydrophobic at the AtxA-FXa light chain interface, as compared to 26.4% at the AtxA-FXa heavy chain interface. Overall, 29.7% of the contacts are hydrophobic at the AtxA-FXa interface. These interface regions are identified separately by the protein-protein interface prediction server PPI-

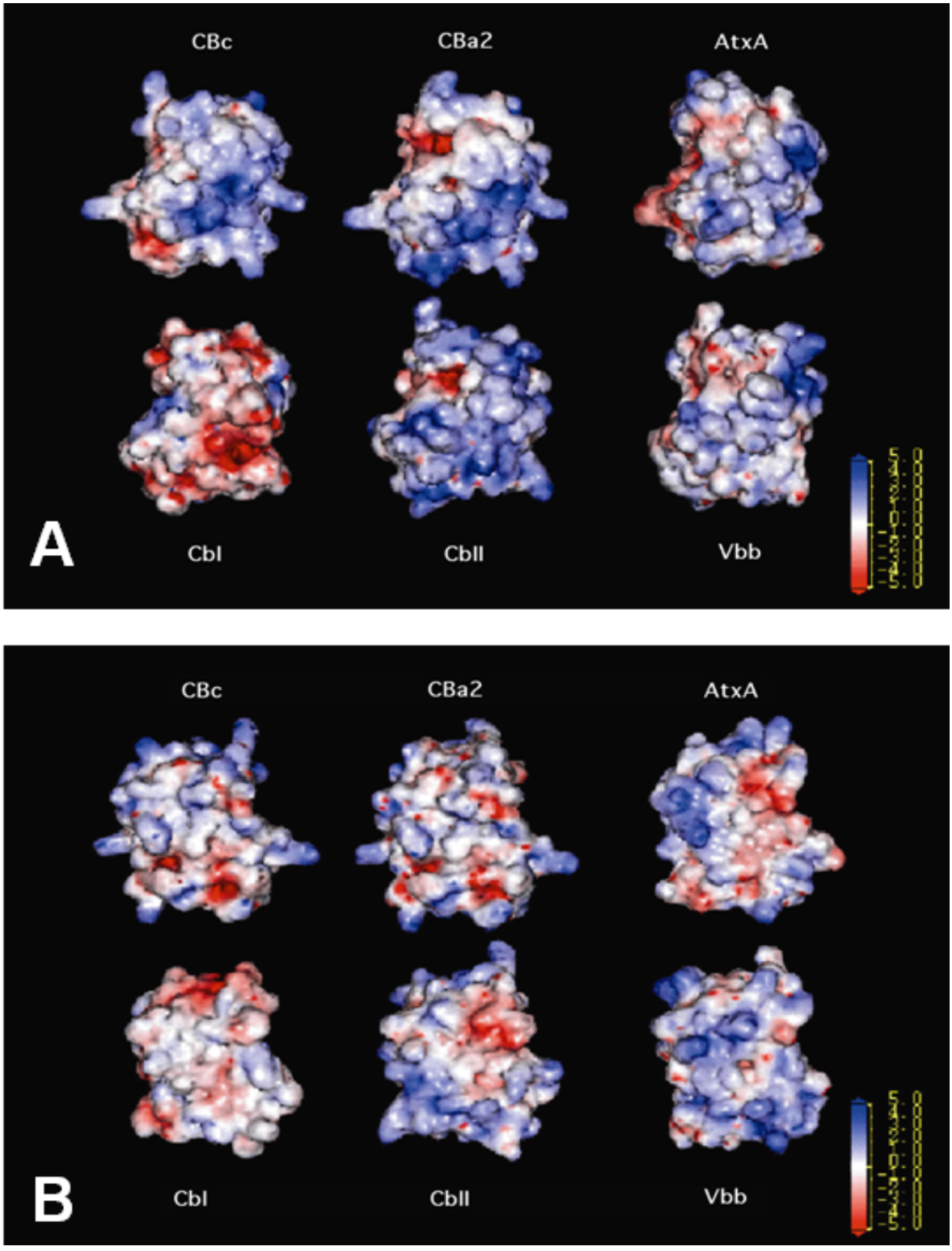

Figure 4
MEP at the solvent accessible surface of the 3D molecular models of the *Viperidae* SVPLA$_2$s. A. The models correspond to CBc, CBa$_2$, AtxA, CbI, CbII, and *Vbb*. Color codes correspond to MEP in kT/e units: blue, +5; red, -5; white, 0. Front view. B. Back view.

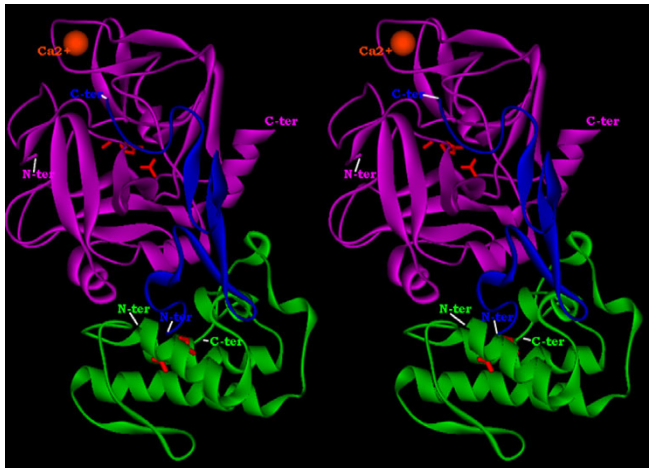

Figure 5
Ribbon representation of the 3D molecular model of the complex between AtxA and the light and heavy chains of FXa. Crossed-eye stereo ribbon representation, with AtxA in green, the light and heavy chains of FXa in blue and purple, respectively. Catalytic site residues are red sticks for both AtxA (His48, Asp99) and FXa (His57, Ser102, Asp195). The metal Ca^{2+} ion of FXa is depicted as an orange sphere. The N- and C-ter of the AtxA, FXa's heavy chain and FXa's light chain are indicated.

Pred. For example, for AtxA, the highest score PPI-Pred patch, which represents the most probable protein-protein binding site, includes helices A and B, the Ca^{2+}-loop, part of the 69-loop, two residues from the front strand of the β-wing, and the four C-terminal residues (results not shown). Fig. 8 shows the regions mapped by docking simulations in the modeled structure of complexed AtxA.

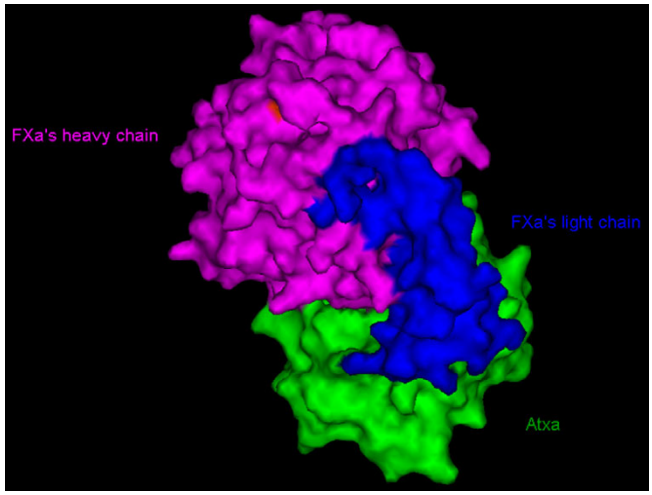

Figure 6
Solvent-accessible surface representation of the 3D molecular model of the complex between AtxA and the light and heavy chains of FXa. Color coding as in Fig. 5.

The first line of Fig. 9A and 9B show the amino acid sequences of the parts of the heavy and light chains of the crystal structure of FXa (PDB 2BOH), detected at the surface respectively. The heavy chain (Fig. 9A) includes the serine proteinase catalytic domain of FXa (catalytic-site residues in bold), and the light chain (Fig. 9B) includes the EGF-like 2 domain. The following lines in Fig. 9A and 9B show the FXa residues at the interface of the docked FXa-$SVPLA_2$ complexes (residues appearing three or more times). The regions of FXa at the interface with CBc, MtxII, CbII, AtxA and CBa_2 in the resulting docked complexes include, in the light chain (Fig. 9B), the N-terminal region of the EGF-like 2 domain: Arg86-Ser90 and Cys100-Glu102, Gln104, Asn105. In the heavy chain (Fig. 9A), they include the following regions. Region I: Arg93; Phe101 (from the 99-loop). Region II: Arg125; Asp126; Glu129-Ser130; Thr134. Region III: Tyr162; Asp164-Asn166; Lys169; Leu170. Region IV: Gln178 and Asn179 (from the 174-loop). Region V: Lys230, Thr232, Ala233, Phe234 and Lys236 (all residues from the C-terminal helix). Fig. 10 shows these regions in the 3D model of complexed FXa. Some of these residues belong to loops surrounding the catalytic-site cleft.

We show in Fig. 11A and 11B the intermolecular residue contacts for the AtxA-FXa interface for which the contact area is equal to or greater than 10 $Å^2$. We observe from this map that the heavy chain of FXa interacts with the following regions of the PLA_2: a portion of the Ca^{2+} loop, the helix C-β-wing loop, and the C-terminal segment (including Lys127, which has an effect in the binding to FXa) (Fig. 11A). The light chain of FXa establishes intermolecular contacts with the remaining regions: helices A and B, and the β-wing (Arg77) of AtxA (Fig. 11B). From the CSU analysis of interfaces, it follows that the contacts between $SVPLA_2$ and FXa are of diverse nature -aromatic-aromatic, hydrophobic-hydrophobic, salt bridges and H-bonds. There are also destabilizing hydrophobic-hydrophilic interactions. Few of the contacts take place between same-nature residues, like Lys127 from AtxA and Arg93 from FXa's heavy chain (Fig. 11A). These contacts are between non-polar atoms or between non-polar and polar atoms of side chains at the surface of the molecules, where the presence of the aqueous solvent can buffer the electrostatic interactions.

Discussion

Existence of different anticoagulant mechanisms

The classification of the anticoagulant potency (strong, weak, non-anticoagulant) of a $SVPLA_2$ depends on the anticoagulant assay used and on whether this assay leads to establishing the mechanism of action. Usually, the

```
                                                                  50
CBc M18     HLLQFNKMIKFETRKNAIPF-YAFYGCYCGWGGRGRPKDATDRCCFVHDC
MtxII M10   SLFELGKMILQETGKNPAKS-YGAYGCNCGVLGRGKPKDATDRCCYVHKC
CbII M20    NLFQFTKMINGKLGAFAVLN-YISTGCYCGWGGQGTPKDATDRCCFVHDC
AtxA M7     SLLEFGMMILGETGKNPLTS-YSFYGCYCGVGGKGTPKDATDRCCFVHDC
CBa2 M17    SLLQFNKMIKFETRKNAVPF-YAFYGCYCGWGGQGRPKDATDRCCFVHDC
hsPLA2      NLVNFHRMIKLTTGKEAALS-YGFYGCHCGVGGRGSPKDATDRCCVTHDC

                                                                 100
CBc M18     CYG---KLAKC-----NTKWDIYPYSLKSGYITC-GKGTWCEEQICECDR
MtxII M10   CYK---KLTGC-----NPKKDRYSYSWKDKTIVC-GENNSCLKELCECDK
CbII M20    CYG---RVKGC-----NPKLAIYSYSFQKGNIVC-GKNNGCLRDICECDR
AtxA M7     CYG---NLPDC-----SPKTDRYKYHRENGAIVC-GKGTSCENRICECDR
CBa2 M17    CYG---KLAKC-----NTKWDIYRYSLKSGYITC-GKGTWCKEQICECDR
hsPLA2      CYKRLEKRG-C-----GTKFLSYKFSNSGSRITCAK-QDSCRSQLCECDK

                                                          133
CBc M18     VAAECLRRSLSTYKYGYMFYPDSRC-RGPSETC
MtxII M10   AVAICLRENLNTYNKKYRYYLKPLC--KKADAC
CbII M20    VAANCFHQNKNTYNRNYRFLSSSRC-RQTSEQC
AtxA M7     AAAICFRKNLKTYNYIYRNYPDFLC-KKESEKC
CBa2 M17    VAAECLRRSLSTYKNEYMFYPDSRC-REPSETC
hsPLA2      AAATCFARNKTTYNKKYQYYSNKHCRGSTPRC
```

Figure 7

***Viperidae SVPLA$_2$* interface amino acid residues.** Interface amino acid residues of the SVPLA$_2$ complexes with FXa (CBc, MtxII, CbII, AtxA and CBa$_2$). Underlined characters denote residues identified by mutagenesis to be critical for binding to FXa and inhibition of prothrombinase activity [39, 51]. Bold characters denote residues defining the IBS of hsPLA$_2$ [13, 14]. Cyan-shadowed characters denote residues found at the interface of the selected complexes. The alignment reflects Renetseder's numbering system.

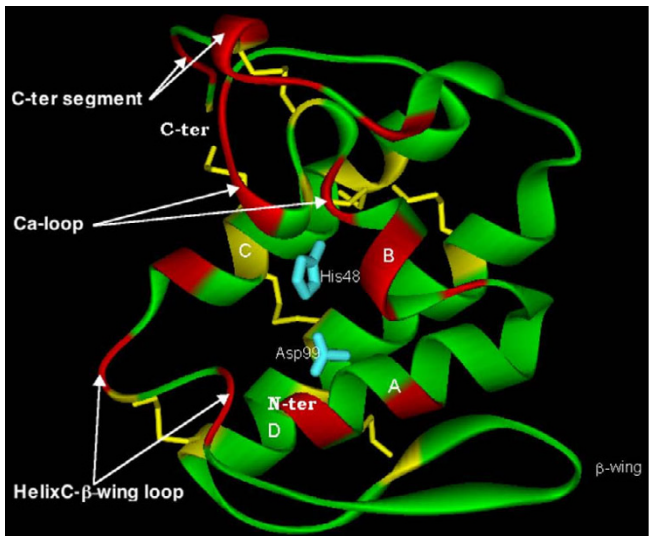

Figure 8

Ribbon diagram of the molecular model of AtxA showing the identified interface regions. The identified interface regions in SVPLA$_2$s from Fig. 7 and made up of consensus positions 2, 3, 7 (helix A); 16; 18, 19 (helix B); 23, 24; 31–34 (Ca^{2+} loop); 53, 59, 60, 69, 70 (helix C-β-wing loop); and 118, 119, 121–124, 129–131, 133 (C-terminal segment), are in red (see Results section).

recalcification time assay, one of the simplest assays, is used. This method is very sensitive to the lipid levels in the plasma but does not show whether the mechanism is PL-independent or not. Our results deal with the interaction of anticoagulant PLA$_2$s with FXa through the non-catalytic, PL-independent mechanism of action and are to be compared to studies performed under the same conditions. As mentioned before, only three PLA$_2$s -CM-IV of *N. nigricolis*, AtxA of *V. ammodytes ammodytes*, and hsPLA$_2$- have been studied under these conditions. In this work, we complete these studies by testing several other SVPLA$_2$ from *Viperidae* venom. Our results clearly show that CBc and MtxII interact with FXa with very high affinity and strongly inhibit the formation of the prothrombinase complex. CbII, AtxA and CBa$_2$ possess good affinity for FXa and good anticoagulant potency. VRV-PLVIII, *bAhp* and *Vbb* possess weak affinity for FXa and show weaker inhibition of prothrombinase activity. Some of these enzymes (CB, AtxA) also inhibit prothrombinase activity in the presence of PL (not shown). AGTX, the CA subunit of CTX, *Catx* and CbI do not interact with FXa and do not inhibit prothrombinase activity in the absence of PL. Therefore, AGTX, described previously as a weakly anticoagulant PLA$_2$ [38], and VRV-PLVIII, described previously as strongly anticoagulant [74], appear to inhibit blood coagulation through different mechanisms.

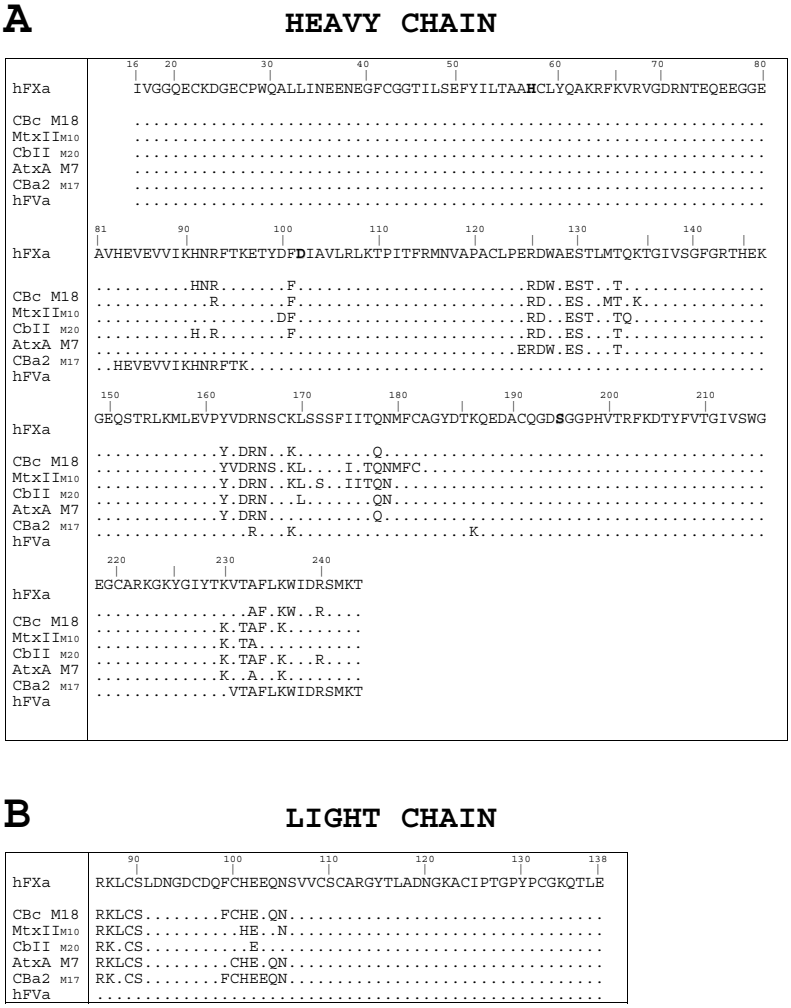

Figure 9

FXa interface amino acid residues. A. Amino acid residues of the heavy chain of FXa at the interface of the selected docked complexes for each SVPLA$_2$. The sequence of FXa shows only residues detected in the X-ray experiment. The last line shows the experimentally reported residues of FXa involved in the binding to FVa [2, 78, 79, 83]. We use Renetseder's notation for the SVPLA$_2$s and chymotrypsinogen notation for FXa. The sequences of CBc, AtxA, CbII and CBa$_2$ were aligned with respect to MtxII. B. Amino acid residues of the light chain of FXa at the interface of the selected docked complexes for each SVPLA$_2$.

Search for an anticoagulant site

Possible location of an anticoagulant site common to Viperidae *SVPLA$_2$s that interact directly with FXa*

Reduced and carboxymethylated CBc did not interact with FXa (Table 1), suggesting that the SVPLA$_2$ needs to adopt the proper conformation for the interaction to take place. In agreement and in the context of the PL-independent anticoagulant mechanism, our combined theoretical and experimental approach highlights the presence of an anticoagulant region composed of amino acid residues that come together in space to constitute a conformational epitope situated in the "front" face of the SVPLA$_2$s. These are the solvent-exposed parts of helix A, helix B, the Ca^{2+} loop, the helix C-β-wing loop, the front strand of the β-wing, and the C-terminal segment of the PLA$_2$ (Fig. 8). Of course, the detailed distribution and composition of those residues varies for each of the SVPLA$_2$s.

Carredano *et al.*[52] determined the 3D structure of group II A monomeric PLA$_2$ RVV-VD from *Vipera r. russelli* (PDB 1VIP), described as a strongly anticoagulant SVPLA$_2$. The authors proposed a site responsible for the strong anticoagulant properties of the toxin, consisting of Glu53, together with a positively charged ridge of non H-bonded lysine residues free for intermolecular interactions in the 53–70 region (Lys60 in RVV-VD and in CBa$_2$). On

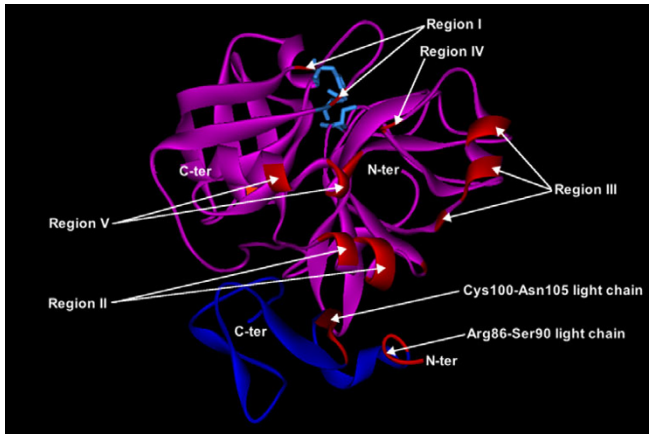

Figure 10
Ribbon diagram of the crystal structure of FXa (PDB 2BOH) showing the identified interface regions. The figure highlights in red the regions corresponding to the identified interface residues from Fig. 9A and B. In the light chain: Arg86-Ser90 and Cys100-Asn105. In the heavy chain: Region I: Arg93; Phe101 (from the 99-loop). Region II: Arg125; Asp126; Glu129-Ser130; Thr134. Region III: Tyr162; Asp164-Asn166; Lys169; Leu170. Region IV: Gln178 and Asn179 (from the 174-loop). Region V: Lys230, Thr232, Ala233, Phe234 and Lys236 (residues from the C-terminal helix). Only residues present three or more times in the same column in the sequences are included. Light chain is in blue, heavy chain in purple. FXa is rotated 90° in a clockwise sense about its vertical axes with respect to Fig. 5. The terminal ends of FXa's chains are labeled. The catalytic triad is represented as cyan sticks.

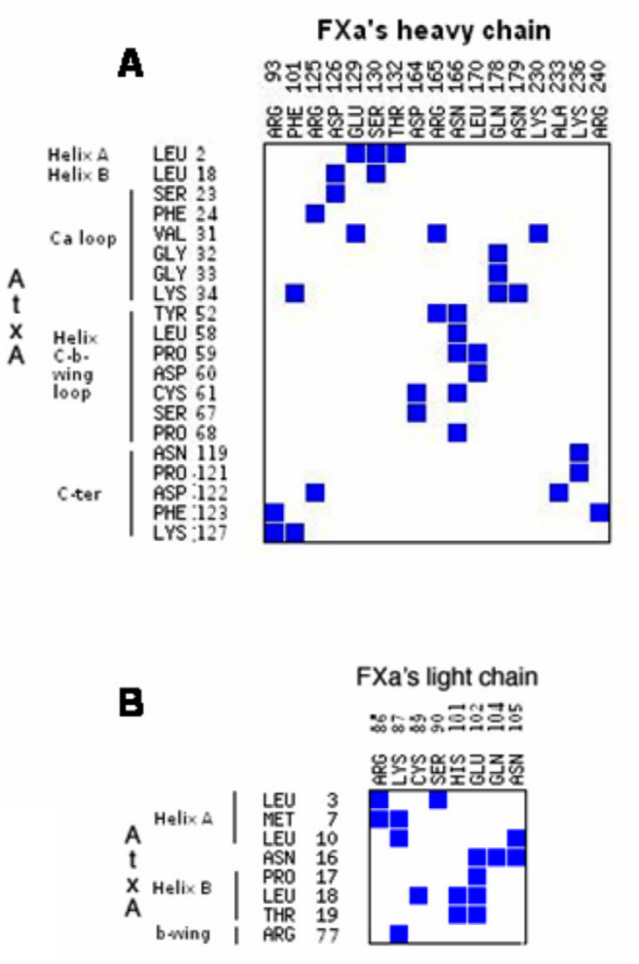

Figure 11
Contact map for the AtxA-FXa complex. A. Heavy-chain FXa residues. Only residues for which the contact area is equal or greater than 10 Å^2 are shown.B. Light-chain FXa residues.

another hand, Zhao *et al.*[75] suggested that residues Trp70 and Glu53 in *bAhp* might play an important role in the anticoagulant activity of the basic SVPLA$_2$s. The study of Zhong *et al.*[76], who tested the anticoagulant potency of *bAhp* mutants, revealed that the Glu53Gly and Trp70Met mutants lost their effects on blood clotting, while Thr56Lys and Asp67Lys had enhanced activity. The reported residues fall in the 53–70 interface region detected in our docked complexes of the strong FXa binders CBc, MtxII, CbII, AtxA and CBa$_2$ (Fig. 8). The possible contribution of Trp70 to the strong anticoagulant activity of PLA$_2$s has also been proposed elsewhere [48]. Nevertheless, the anticoagulant region cannot be localized solely to the 53–70 segment, since enzymes that bind weakly or not at all to FXa contain also basic residues in this region.

The natural mutants CBc and CBa$_2$ present two Gly -> Glu mutations in the C-terminal region (Gly116Glu, Gly128Glu) leading to increases in the IC$_{50}$ values for inhibition of prothrombinase activity of CBa$_2$ with respect to CBc. This is consistent with the results of our sequence comparison analysis, in which we detect the acidic residue at position 128 as characteristic of the NB group, and with the docking results that point to this region as being at the interface of the complexes.

On the other hand, we localized in the crystal structure of hsPLA$_2$ (PDB 1BBC) the mutations that showed the major effects in the inhibition of prothrombinase activity and FXa-binding kinetic parameters [51]. Residues Arg7, Lys10 and Lys16 (helix A) are exposed to the solvent and form a cluster. Residue Lys38 (loop on N-terminus of helix B), and residues Lys123 and Arg126 form another cluster (underlined residues Fig. 7). As expected, the two clusters are situated on the front face and are oriented 180° about this convex surface. They act cooperatively in the binding to FXa. Lys86 carries with it an effect on IC$_{50}$,

but is in the end of the second strand of the β-wing ("back" face) of hsPLA$_2$, indicating that its effect on IC$_{50}$ is not due to the residue being at the interface. No effects are reported dealing with the Ca^{2+} loop and the front strand of the β-wing does not appear in hsPLA$_2$ (Fig. 7); however, to our knowledge, these regions have not yet been probed.

Lastly, our experimental data suggest that the CB-FXa interaction site is different from the CB-CA interface and show that the interaction between FXa and CTX proceeds through a transient ternary (CA, CB, FXa) complex (Fig. 1).

The FXa binding region of PLA$_2$ involves also hydrophobic residues

hsPLA$_2$ contains an unusually large number of prominent cationic patches on its molecular surface, some of which lie on the putative IBS [14], in contrast to bovine pancreatic PLA$_2$ and the SVPLA$_2$ from *Agkistrodon p. piscivorus*, which display only a limited number of such patches [10]. Given the charged nature of the residues critical for binding hsPLA$_2$ and AtxA to FXa, it is clear that electrostatic interactions play a role in the binding. Indeed, the electrostatic asymmetry showed by the MEP calculations must be enhanced by the presence of the essential Ca^{2+} cofactor ion [77] and may be at the origin of the increased affinity of hsPLA$_2$ for FXa in the presence of Ca^{2+} [50]. Thus, long distance electrostatic forces operating at the molecular surface are important and may optimally orient the molecules before binding to FXa. However, electrostatic interactions might not exclusively drive binding to FXa by the *Viperidae* SVPLA$_2$s, as in hsPLA$_2$. Indeed, in addition to basic residues, hydrophobic and aromatic residues play also key roles in optimizing the interaction between SVPLA$_2$s and FXa, given that a ring of hydrophobic residues surrounds the opening to the catalytic site cavity. Thus, for AtxA, many hydrophobic residues (Leu2, 3, 10, 18 and 58; Pro17, 59, 68 and 121; Val31), most of which are located in the N-terminal region, and several aromatic residues (Phe24 and 123; Tyr52) are part of the surface presented to FXa (Fig. 7). Lastly, even though a Phe24Ala mutation in AtxA was not found to change the FXa-binding kinetic parameters [39], we emphasize the need to probe other residues belonging to the hydrophobic ring.

The PLA$_2$ binding region of FXa involves both, the light and heavy chains but not the catalytic site

On our results, the catalytic site of FXa is free and not involved in the interface, in agreement with the conservation of the serine-proteinase catalytic activity after binding by SVPLA$_2$ [51]. Our AtxA-FXa complex shows that one region of the light chain of FXa is involved in the binding to the SVPLA$_2$ and that the N-terminus of the EGF-like 2-domain is pointing south (Fig. 5). Therefore, the EGF-like 1-domain, not visible in the crystal structure of FXa, can interact with the front edge of the β-wing of the PLA$_2$. The Gla domain of FXa (bound to the N-terminus of the EGF-like 1-domain), is well beyond reach in space and not in contact with the PLA$_2$. These two features are in agreement with experimental and biochemical data which support the conclusion that the Gla domain is needed rather for insertion into the PL membrane [51], and with a model of the entire FXa. Indeed, based on the crystal structure of the Gla domain of bovine prothrombin and the NMR coordinates of the bovine FX EGF1 domain, Bajaj and coworkers [2] proposed a model structure for the entire FXa molecule, based upon the crystal structure of porcine FIXa. The EGF domains in the model are oriented south and thus capable of establishing contacts with the β-wing of the PLA$_2$.

Based on the ability of synthetic peptides from FXa to inhibit FXa-induced clotting, a number of authors have reported the FVa binding sites on FXa. The last line of Fig. 9A shows the experimentally reported residues of the heavy chain of FXa incontrovertibly involved in the binding to FVa. These residues are: FXa(His83-Lys96) [78]; FXa(Arg165, Lys169) [79-81]; the 185–189 loop, i.e., FXa(Lys186) [82]; FXa(Val231-Thr244) [83]; and FXa(Arg240) [81]. Three of four of the segments of the catalytic domain of FXa identified to interact with FVa overlap with those identified by us to interact with the *Viperidae* SVPLA$_2$s, namely the segment about Lys90, the 162-loop, and the C-terminal part, about Lys237 (Fig. 9A). This suggests that several residues are shared by both, the SVPLA$_2$-FXa and the FVa-FXa binding interfaces. Moreover, the experimentally identified FXa heavy chain residues involved in binding to FVa are located on the same 3D face of FXa, as in our SVPLA$_2$-FXa complexes.

Arni and coworkers have recently reported the crystal structures of human Gla domainless FXa complexed with two small anticoagulant proteins from a hematophagous nematode [84,85]. The determined exosite from those complexes involves residues from one of the strands of the N-terminal seven-stranded β-barrel (strand β6, residues 80–93) and from the short C-terminal α-helix (residues 233–243) of the catalytic subunit of FXa. Several of these residues fall in regions I and V mapped in our complexes with the SVPLA$_2$s (Fig. 9A and 10).

Several IBS residues are part of the PL-independent anticoagulant site of SVPLA$_2$

By combining the residues defining the IBS [13,14] with the site-directed mutagenesis experiments for probing the basic residues of hsPLA$_2$ involved in binding to FXa[51], we deduce that IBS residues Arg7 and Lys10 bind to FXa.

By homology with hsPLA$_2$, the presumed IBS amino acid residues for AtxA are Leu3, Leu18, Phe24, Lys74 and

Tyr113. On one hand, Lys74, experimentally found to be critical for binding of AtxA to FXa [39], belongs to the IBS. On the other hand, our simulations indicate that IBS residues Leu3, Leu18 and Phe24 are in contact with FXa. In conclusion, several IBS residues are part of the PL-independent anticoagulant site and participate in formation of the complex with FXa.

SVPLA$_2$ are multifunctional proteins with multiple pharmacological sites

The *Viperidae* SVPLA$_2$s studied here are multifunctional proteins, raising the possibility of overlapping or multiple pharmacological sites distinct from the catalytic site[86]. One team[52] has suggested that the neurotoxic site of group II neurotoxic enzymes overlaps with the anticoagulant region. Thus, from the mutants used to test the anticoagulant potency [39] and the neurotoxic function [87] of AtxA, it appears that several residues in the C-terminus are clearly shared by both functions. The overlapping of pharmacological sites is most easily understood in terms of the small size of this family of proteins.

Conclusion

In this paper, we concentrated our efforts on identifying the anticoagulant *Viperidae* SVPLA$_2$s that inhibit blood coagulation via a non-enzymatic, PL-independent mechanism through direct binding to human FXa. Using SPR technology, we showed that CBc and MtxII bind to FXa with the highest affinity and inhibit strongly the prothrombinase complex, whereas CbII, AtxA and CBa$_2$ bind with good, but lesser affinity.

Of the eight mutations that differentiate CBc from CBa$_2$, Arg34Gln in the Ca^{2+} loop and Gly128Glu in the C-terminal segment fall in our identified interface regions; Gly116Glu is just borderline to the C-terminal fragment. Thus, the disappearance of a positive charge and the appearance of two negative charges in this region account for the loss of affinity of CBa$_2$ for FXa with respect to CBc. This is consistent with our consensus sequence analysis, which had associated the presence of Glu at position 128 to a decrease in affinity.

The molecular electrostatic potential we calculate at the surface of the 3D molecular models shows a correlation with the anticoagulant potency of the SVPLA$_2$s. However, since not all basic PLA$_2$ are strong anticoagulants [44], the basic character of the PLA$_2$ seems to be a necessary but not sufficient condition for its anticoagulant potency.

Mapping of the FXa-interface zone in the 3D structures of the SVPLA$_2$s by binding-site directed docking simulations, allowed us to detect several FXa-binding regions that come together to form a conformational epitope on the "front" surface of the SVPLA$_2$s. One of the regions maps to the 53–70 segment, proposed in the past to be the anticoagulant region. According to our findings, this region is to be extended, on one hand, to helices A and B and to the "front" strand of the β-wing, and to the Ca^{2+} loop and the C-terminal direction, on the other. The FXa interface forms a novel exosite that involves both, the light and heavy chains.

Our work epitomizes the use of binding affinity and mutational experimental data in guiding molecular docking simulations by indicating which species associate and then outlining the possible interacting surface patches.

Finally, there has been intense interest in the development of FXa inhibitors for the treatment of thrombotic diseases. Anticoagulant *Viperidae* SVPLA$_2$s, which interact with FXa via a non-catalytic, PL-independent mechanism, represent a novel family of selective FXa inhibitors. Structural information on the binding of these PLA$_2$ to FXa should be useful in the 3D structure-based design of therapeutic agents. The synthesis of peptides or peptidomimetics derived from our mapped regions could lead to the development of new antithrombotic molecules capable of delaying *in vivo* the activation stage of the prothrombinase complex and to their use as supplementary agents in antithrombotic therapy.

Methods

Reagents including Sensor Chips CM5, surfactant P20, the amine coupling kit containing *N*-hydroxysuccinimide (NHS), *N*-ethyl-*N*'-(3-diethylaminopropyl)carbodiimide (EDC) and ethanolamine hydrochloride were supplied by Biacore (Biacore AB, Uppsala, Sweden). All other chemicals and solvents of the highest available purity were obtained from either Merck A.G. (Darmstad, Germany), Prolabo (Paris, France) or Sigma Co (St. Louis, MO, USA). CbI and CbII from *Pseudocerastes fieldi* venom were supplied by Dr. A. Bdolah (Dept. of Zoology, Tel Aviv University, Israel) [88]. AtxA from *Vipera ammodytes ammodytes* was purchased from Latoxan. Recombinant hsPLA$_2$ was produced in our laboratory as described previously[89]. Isoforms of the CB subunit of crotoxin (CBa$_2$ and CBc), isoform CA$_2$ of the acidic subunit of crotoxin, and the VRV-PLVIII from *Daboia russelli pulchella* venom were purified in our laboratory as described previously [55,56,62,67]. CBc was reduced by dithiothreitol and alkylated with iodoacetic acid according to the procedure described by Faure *et al.*[56]. Drs. I. Krizaj (Institute Jozef Stefan, Ljubliana), E. Myatt (Argon Institute), Y. C. Chen (Institut of Biochemistry, Shanghai, China), and J. Perales (Fundaçao Oswaldo Cruz, Rio de Janeiro, Brazil) provided PLA$_2$ from *Vipera berus berus*, PLA$_2$ from *Crotalus atrox*, AGTX and the basic PLA$_2$ from *Agkistrodon hallys pallas*, and MtxII from *Bothrops asper*, respectively. We purchased human activated blood coagulation factor (FXa)

from Enzyme Res. Laboratories, USA (MW 46 kDa). The corresponding amino acid sequence shows a Glu residue at position 150 of the heavy chain, whereas UniProt's entry P00742 (FA10_HUMAN) shows an Arg. This residue is at the surface of the molecule. For the simulations, we chose the 2.2 Å resolution crystallographic structure of Gla-domainless FXa from entry 2BOH [90] of the PDB, which corresponds to sequence FA10_HUMAN and is made up of the heavy chain and of the EGF-like 1 and 2 domains of the light chain. Only light chain residues Arg86-Glu138, which represent the EGF-like 2 domain, and heavy chain residues Ile16-Thr244 are located in the X-ray diffraction experiment -the entire EGF-like 1 domain and its hydrophobic peptide preceding it being disordered. In this structure, FXa is co-crystallized with a 2-carboxyindole inhibitor and a Ca^{2+} ion chelated by Asp70, Asn72, Gln75 and Glu80 of the catalytic (heavy) chain. We removed the inhibitor and the water molecules for the calculations.

We performed computer graphics using PyMOL (DeLano Scientific LLC, San Francisco, CA, USA), and the insightII and DS Visualizer softwares (Accelrys Inc, San Diego, CA, USA). Computer calculations were performed with the insightII software package on SGI graphic stations and using programs available in servers in the World Wide Web with PC workstations.

Determination of prothrombinase activity

We determined the anticoagulant potency of the $SVPLA_2$s by measuring *in vitro* the inhibition of prothrombinase activity (IC_{50}). We used an *in vitro* biological test in which the prothrombinase complex was reconstituted at 37°C from purified human factors FVa and FXa in the presence of Ca^{2+}, but without the addition of PL[39]. The purified prothrombinase components (FVa 10 nM, FXa 10 nM, and different concentrations of $SVPLA_2$: 0, 10, 20, 50, 100, 200, 500 nM) were incubated 5 min at 37°C in Tris-buffered saline (0.05 M Tris/HCl, 0.1 M NaCl, 0.5% BSA, 5 mM $CaCl_2$, pH 7.4). The reaction was then started with 110 nM prothrombin. We measured activated prothrombin activity every 20 min, as described previously [50], with small modifications. We determined the IC_{50} value, which corresponds to 50% inhibition of thrombin generation for the different $SVPLA_2$s in the absence of PL.

Surface Plasmon Resonance studies

We analyzed of the interaction between the $SVPLA_2$s from the *Viperidae* family, and FXa by SPR using a BIACORE® 2000 system (Biacore AB, Uppsala, Sweden). The running and dilution buffer in all experiments was Hepes (HBS; 10 mM Hepes, 150 mM NaCl, 5 mM $CaCl_2$, 0.005% surfactant P20, pH 7.4). The experiments were conducted at 37°C. Human FXa was covalently coupled via primary amino groups on a CM5 sensor chip surface according to Prijatelj *et al.*[39]. One independent flow cell of the same sensor chip was used as a control flow cell and was subjected to a "blank immobilization," i.e., with no FXa added. We found the SPR signal for immobilized FXa on three different flow cells to be 1500 RU, 3000 RU and 5840 RU (1 RU corresponds to 1 pg/mm^2 of immobilized protein). We injected PLA_2 samples (0, 0.25, 0.5, 1, 2, 4, and 8 μg/ml) at 37°C with a flow rate of 20 μl/min on independent runs on the control and assay flow cells and their binding was monitored. Between each injection, we regenerated surfaces with twice 5 μL of 1 M NaCl. The apparent equilibrium constant, $\langle K_d^{app} \rangle = \langle k_{off} \rangle / \langle k_{on} \rangle$, the average dissociation rate constant $\langle k_{off} \rangle$ and the average association rate constant $\langle k_{on} \rangle$ were calculated using Biacore's BIAevaluation 3 software. The kinetic models used to fit the data included the Langmuir association, heterogeneous analyte and conformational change. Only the first one showed the lowest closeness-of-fit value (χ^2). In addition, the other models resulted in affinities much lower (μM) than expected (nM).

Sequence homologies and alignments

The sequence databases and identifiers are the following: CBc (also known as CB1), Uniprot P62022; CBa_2 (also known as CB2), P24027; AGTX, P14421; AtxA, P00626; MtxII, P24605; *Vbb*, P31854; CbI, gi 1345182 [57]; CbII, gi 1345181 [57]; CA, isoform CA_2 [56](obtained by post-translational modification of ProCA, P08878).

For sequence alignments, we used the LALIGN program [91,92], which finds multiple matching sub-segments in two sequences and shows the local sequence alignments. For representing sequences and their alignments, we used Weblogo, a web-based application designed to generate sequence logos [93,94].

Molecular modeling

Given the high sequence homology between the $SVPLA_2$s and diverse PLA_2s whose crystal structures are available, we applied homology modeling to generate 3D model structures of the $SVPLA_2$s using the Biopolymer and Homology modules of the insightII software package (Accelrys Inc. San Diego, CA, USA). We retrieved the PLA_2s of the template proteins of known 3D structure from the Protein Data Bank[95]. The template proteins are: AGTX, the neutral PLA_2 from *Agkistrodon halys pallas*[96] (PDB **1A2A**); VRV-PLVIII, the PLA_2 from *Daboia russelli pulchella*[97] (PDB **1FB2**); MtxII, myotoxin II, a K49-PLA_2 from *Bothrops asper*. [98] (PDB **1CLP**); the PLA_2 from *Crotalus atrox*[99] (PDB **1PP2**); the PLA_2 from *Vipera russelli russelli*[52] (PDB **1VIP**) and *bAhp*, the basic PLA_2 from *Agkistrodon halys pallas* [100] (PDB **1JIA**).

After building the structurally conserved regions (SCR) and the structurally variable regions (SVR), we replaced

the side chains of the template protein by the target protein's side chains in a predetermined library conformation. We then performed a rotamer search assignment in order to avoid atomic steric clashes and optimize the inter-residue energies. We included a structurally conserved catalytic water molecule during the modeling. We did not model the Ca^{2+} ion at the Ca^{2+} binding site, since it is absent in several X-ray structures. We subjected the obtained models to an overall internal energy minimization using the CFF91 force field. The protonation state of ionizable side chains and of the N- and C-termini was set for pH 7. Atomic partial charges were those of the CFF91 field. We used a distance-dependent dielectric function of 4r. We applied the cell multipole summation method for van der Waals and coulomb interactions. We used none of the cross terms of the force field. We applied the same conditions to the amino acid residues in the crystal structures used. We checked the stereo chemical quality of the models with the Struct_Check program, and the correctness of the folding with the Profiles3D Verify functionality (self-compatibility scores, insightII). The amino acid residue numbering is based on that of Renetseder *et al.*[15].

Molecular Electrostatic Potential

The MEP is generated by the combined presence of all partial charges residing on the atoms as a function of their positions. The potential was calculated with the DelPhi 2.5 program in insightII. The grid resolution was of 0.833 Å/grid point. The interior and exterior dielectric constants were 2 and 80, respectively. The value of the ionic strength was 0.145; the probe radius was 1.4 Å and the ionic radius 2.00 Å. The treatment of the grid points at the boundary used a full Coulomb approximation. The values of the potential are given in kT/e units at T = 298 K.

Molecular docking. Protein interfaces and interface contacts

We generated the molecular complexes with the PatchDock rigid body molecular docking procedure[101]. Given two molecules, the surfaces of the molecules to dock are divided by PatchDock into patches according to the surface shape. These patches correspond to patterns that visually distinguish between puzzle pieces. We used a clustering RMSD criterion of 4.0 Å. The output lists the rank of the complex and its approximate interface area. We selected PatchDock for the docking simulations since it allows *a priori* focusing on the vicinity of potential binding sites. In other words, it is possible to upload a receptor-binding site and a ligand-binding site. We took the $SVPLA_2$s as the "receptor" molecules and FXa as the "ligand" molecule.

Thus, we generated molecular complexes only for those $SVPLA_2$s for which we find experimental evidence of biophysical interaction, i.e., in which the binding affinity between the PLA_2 and FXa, as measured by SPR, was high. In addition, we used the available mutagenesis data for AtxA[39] to filter the docked complexes so that AtxA residues that show a decrease in the binding affinity for FXa are at the interface of the complex and define a binding site. The residues defining the binding site on AtxA are Arg72, Lys74, His76 and Arg77 (front edge of the β-wing), and Arg118, Lys127, Lys128 and Lys132 (C-terminal fragment)[39]. We defined no ligand-binding site for FXa.

From the candidate complexes generated by PatchDock for AtxA, only one showed a binding mode compatible with the ensemble of the mutagenesis data -many complexes showed binding to either the β-wing or the C-terminal fragment of the $SVPLA_2$ or other regions of the AtxA. Thereafter, we selected those complexes for the other $SVPLA_2$s that showed the same binding mode as AtxA and whose Cα RMSDs with respect to the AtxA-FXa complex were minimal. After generation of the complexes, we used the "move apart" option of PatchDock, which separates (by 1.6 Å) the receptor and ligand subunits in order to eliminate steric hindrances at the interface. We further improved the fitting of the complex by applying firstly the SCWRL3 side chain modeling procedure [102], in which we froze all disulfide bonds, as well as the side chains of heavy chain residues Asp70 and Glu80, which chelate the Ca^{2+} ion in FXa. After the rotamer search, we applied additional energy minimizations in order to reach a minimal internal energy conformation. The entire approach assumes that no drastic conformational changes occur during complexation.

On another hand, we submitted the $SVPLA_2$ models to the Protein-Protein Interface Prediction (PPI-Pred) server [26,103] to predict their binding sites. PPI-Pred predicts protein-protein binding sites using a combination of surface patch analysis and a support vector machine trained on 180 proteins involved in both obligate and non-obligate interactions.

The interface between the two polypeptide chains of each of the complexes was characterized with the Protein interfaces, surfaces and assemblies service PISA [104,105]. The interface contacts were obtained through a contact map analysis and characterized with the SPACE bioinformatics tools CMA (Contact Map Analysis) and CSU (Contacts of Structural Units) [106,107]. We show only interface contacts for which the contact area is equal to or greater than 10 $Å^2$.

Abbreviations

AGTX: agkistrodotoxin, the neurotoxic, neutral PLA_2 from *Agkistrodon halys pallas* venom

bAhp: the basic PLA_2 from *Gloydious* (*Agkistrodon) halys pallas* venom

AtxA: isoform A of ammodytoxin from *Vipera ammodytes ammodytes* venom

CA_2: one of the isoforms of the acidic subunit of crotoxin

CBa_2, CBc: isoforms of the basic subunit of crotoxin

CbI: the α isoform of the acidic subunit of the CbI-CbII complex from *Pseudocerastes fieldi* venom

CbII: the basic subunit of the CbI-CbII complex from *Pseudocerastes fieldi* venom

CTX: crotoxin, β-neurotoxin from *Crotalus durissus terrificus* venom, made of acidic CA and basic CB subunits

CbI-CbII: β-neurotoxin from *Pseudocerastes fieldii* venom, composed of CbI and CbII subunits

FVa: Activated human coagulation factor V

FXa: Activated human coagulation factor X, also known as Stuart factor or Stuart-Prower factor

$hsPLA_2$: Non-pancreatic secreted human group IIA phospholipase A_2

IBS: Interfacial Binding Site

$<k_{on}>$: average association rate constant

$<k_{off}:>$: average dissociation rate constant

$<K_d{}^{app}>$: average apparent dissociation constant = $<k_{off}>/<k_{on}>$

MtxII: Myotoxin II from *Bothrops asper* venom

PL: Phospholipids

Vbb: the PLA_2 from *Vipera berus berus* venom

Catx: the PLA_2 from *Crotalus atrox* venom

RU: Resonance units

$sPLA_2$: Secreted phospholipase A_2

SPR: Surface plasmon resonance

$SVPLA_2$: Group IIA snake venom secreted phospholipase A_2

VRV-PLVIII the PLA_2 from *Daboia russelli pulchella* venom

Authors' contributions

GF and RCM conceived the study, analyzed the results and wrote the manuscript. All authors performed the research. In particular, GF carried out SPR affinity measurements, prothrombinase inhibition experiments, and purification and carboxymethylation of PLA_2s; VTG assisted in purification of PLA_2 and participated in SPR studies and discussions; RCM carried out sequence analysis, molecular modeling and docking simulations.

Acknowledgements

This work was carried out in part in the Unité des Venins (Institut Pasteur), directed by Dr. Cassian Bon. We sincerely thank Dr. Graham Bentley for critical reading of the manuscript.

References

1. Davie EW: **Biochemical and molecular aspects of the coagulation cascade.** *Thromb Haemost* 1995, **74(1):**1-6.
2. Sabharwal AK, Padmanabhan K, Tulinsky A, Mathur A, Gorka J, Bajaj SP: **Interaction of calcium with native and decarboxylated human factor X. Effect of proteolysis in the autolysis loop on catalytic efficiency and factor Va binding.** *J Biol Chem* 1997, **272(35):**22037-22045.
3. Greer J: **Comparative modeling methods: application to the family of the mammalian serine proteases.** *Proteins* 1990, **7(4):**317-334.
4. Perona JJ, Craik CS: **Structural basis of substrate specificity in the serine proteases.** *Protein Sci* 1995, **4(3):**337-360.
5. Perona JJ, Craik CS: **Evolutionary divergence of substrate specificity within the chymotrypsin-like serine protease fold.** *J Biol Chem* 1997, **272(48):**29987-29990.
6. Serrano SM, Maroun RC: **Snake venom serine proteinases: sequence homology vs. substrate specificity, a paradox to be solved.** *Toxicon* 2005, **45(8):**1115-1132.
7. Kalafatis M, Egan JO, van 't Veer C, Cawthern KM, Mann KG: **The regulation of clotting factors.** *Crit Rev Eukaryot Gene Expr* 1997, **7(3):**241-280.
8. Nesheim ME, Taswell JB, Mann KG: **The contribution of bovine Factor V and Factor Va to the activity of prothrombinase.** *J Biol Chem* 1979, **254(21):**10952-10962.
9. Berg OG, Gelb MH, Tsai MD, Jain MK: **Interfacial enzymology: the secreted phospholipase A(2)-paradigm.** *Chem Rev* 2001, **101(9):**2613-2654.
10. Han SK, Yoon ET, Scott DL, Sigler PB, Cho W: **Structural aspects of interfacial adsorption. A crystallographic and site-directed mutagenesis study of the phospholipase A2 from the venom of Agkistrodon piscivorus piscivorus.** *J Biol Chem* 1997, **272(6):**3573-3582.
11. Koduri RS, Baker SF, Snitko Y, Han SK, Cho W, Wilton DC, Gelb MH: **Action of human group IIa secreted phospholipase A2 on cell membranes. Vesicle but not heparinoid binding determines rate of fatty acid release by exogenously added enzyme.** *J Biol Chem* 1998, **273(48):**32142-32153.
12. Lin Y, Nielsen R, Murray D, Hubbell WL, Mailer C, Robinson BH, Gelb MH: **Docking phospholipase A2 on membranes using electrostatic potential-modulated spin relaxation magnetic resonance.** *Science* 1998, **279(5358):**1925-1929.
13. Canaan S, Nielsen R, Ghomashchi F, Robinson BH, Gelb MH: **Unusual mode of binding of human group IIA secreted phospholipase A2 to anionic interfaces as studied by continuous wave and time domain electron paramagnetic resonance spectroscopy.** *J Biol Chem* 2002, **277(34):**30984-30990.
14. Snitko Y, Koduri RS, Han SK, Othman R, Baker SF, Molini BJ, Wilton DC, Gelb MH, Cho W: **Mapping the interfacial binding surface of human secretory group IIa phospholipase A2.** *Biochemistry* 1997, **36(47):**14325-14333.
15. Renetseder R, Brunie S, Dijkstra BW, Drenth J, Sigler PB: **A comparison of the crystal structures of phospholipase A2 from**

bovine pancreas and Crotalus atrox venom. *J Biol Chem* 1985, **260(21):**11627-11634.
16. Lambeau G, Lazdunski M: **Receptors for a growing family of secreted phospholipases A2.** *Trends Pharmacol Sci* 1999, **20(4):**162-170.
17. Krizaj I, Gubensek F: **Neuronal receptors for phospholipases A(2)and beta-neurotoxicity.** *Biochimie* 2000, **82(9–10):**807-814.
18. Murakami M, Kambe T, Shimbara S, Yamamoto S, Kuwata H, Kudo I: **Functional association of type IIA secretory phospholipase A(2) with the glycosylphosphatidylinositol-anchored heparan sulfate proteoglycan in the cyclooxygenase-2-mediated delayed prostanoid-biosynthetic pathway.** *J Biol Chem* 1999, **274(42):**29927-29936.
19. Sartipy P, Johansen B, Gasvik K, Hurt-Camejo E: **Molecular basis for the association of group IIA phospholipase A(2) and decorin in human atherosclerotic lesions.** *Circ Res* 2000, **86(6):**707-714.
20. Boilard E, Bourgoin SG, Bernatchez C, Surette ME: **Identification of an autoantigen on the surface of apoptotic human T cells as a new protein interacting with inflammatory group IIA phospholipase A2.** *Blood* 2003, **102(8):**2901-2909.
21. Faure G: **Natural inhibitors of toxic phospholipases A(2).** *Biochimie* 2000, **82(9–10):**833-840.
22. Kini RM: **Structure-function relationships and mechanism of anticoagulant phospholipase A2 enzymes from snake venoms.** *Toxicon* 2005, **45(8):**1147-1161.
23. Faure G: **Different protein targets for snake venom phospholipases A2.** In *Toxines et recherches biomédicales* Edited by: Goudey-Perrière F, Bon C, Puiseux-Dao S, Sauviat M. Paris: Elsevier; 2002:305-313.
24. Huang MZ, Gopalakrishnakone P, Kini RM: **Role of enzymatic activity in the antiplatelet effects of a phospholipase A2 from Ophiophagus hannah snake venom.** *Life Sci* 1997, **61(22):**2211-2217.
25. Kini RM: **Excitement ahead: structure, function and mechanism of snake venom phospholipase A2 enzymes.** *Toxicon* 2003, **42(8):**E827-840.
26. Bradford JR, Westhead DR: **Improved prediction of protein-protein binding sites using a support vector machines approach.** *Bioinformatics* 2005, **21(8):**1487-1494.
27. Tu AT: **Reptile venoms and toxins.** New York: M. Dekker; 1991.
28. Cirino G, Cicala C, Sorrentino L, Browning JL: **Human recombinant non pancreatic secreted platelet phospholipase A2 has anticoagulant activity in vitro on human plasma.** *Thromb Res* 1993, **70(4):**337-342.
29. Inada M, Crowl RM, Bekkers AC, Verheij H, Weiss J: **Determinants of the inhibitory action of purified 14-kDa phospholipases A2 on cell-free prothrombinase complex.** *J Biol Chem* 1994, **269(42):**26338-26343.
30. Boffa GA, Boffa MC, Winchenne JJ: **A phospholipase A2 with anticoagulant activity. I. Isolation from Vipera berus venom and properties.** *Biochim Biophys Acta* 1976, **429(3):**828-838.
31. Boffa MC, Boffa GA: **A phospholipase A2 with anticoagulant activity. II. Inhibition of the phospholiped activity in coagulation.** *Biochim Biophys Acta* 1976, **429(3):**839-852.
32. Stefansson S, Kini RM, Evans HJ: **The basic phospholipase A2 from Naja nigricollis venom inhibits the prothrombinase complex by a novel nonenzymatic mechanism.** *Biochemistry* 1990, **29(33):**7742-7746.
33. Kini RM, Evans HJ: **Structure-function relationships of phospholipases. The anticoagulant region of phospholipases A2.** *J Biol Chem* 1987, **262(30):**14402-14407.
34. Kerns RT, Kini RM, Stefansson S, Evans HJ: **Targeting of venom phospholipases: the strongly anticoagulant phospholipase A(2) from Naja nigricollis venom binds to coagulation factor Xa to inhibit the prothrombinase complex.** *Arch Biochem Biophys* 1999, **369(1):**107-113.
35. Stefansson S, Kini RM, Evans HJ: **The inhibition of clotting complexes of the extrinsic coagulation cascade by the phospholipase A2 isoenzymes from Naja nigricollis venom.** *Thromb Res* 1989, **55(4):**481-491.
36. Teng CM, Chen YH, Ouyang C: **Biphasic effect on platelet aggregation by phospholipase a purified from Vipera russellii snake venom.** *Biochim Biophys Acta* 1984, **772(3):**393-402.
37. Teng CM, Chen YH, Ouyang CH: **Effect of Russell's viper venom phospholipase A on blood coagulation and platelet aggregation.** *Semin Thromb Hemost* 1985, **11(4):**367-372.
38. Kini RM: **Venom phospholipase Ab2 s enzymes: structure, function, and mechanism.** Chichester; New York: John Wiley; 1997.
39. Prijatelj P, Charnay M, Ivanovski G, Jenko Z, Pungercar J, Krizaj I, Faure G: **The C-terminal and beta-wing regions of ammodytoxin A, a neurotoxic phospholipase A2 from Vipera ammodytes ammodytes, are critical for binding to factor Xa and for anticoagulant effect.** *Biochimie* 2006, **88(1):**69-76.
40. Valentin E, Lambeau G: **What can venom phospholipases A(2) tell us about the functional diversity of mammalian secreted phospholipases A(2)?** *Biochimie* 2000, **82(9–10):**815-831.
41. Heinrikson RL, Krueger ET, Keim PS: **Amino acid sequence of phospholipase A_2-alpha from the venom of *Crotalus adamanteus*. A new classification of phospholipases A_2 based upon structural determinants.** *J Biol Chem* 1977, **252(14):**4913-4921.
42. Davidson FF, Dennis EA: **Evolutionary relationships and implications for the regulation of phospholipase A2 from snake venom to human secreted forms.** *J Mol Evol* 1990, **31(3):**228-238.
43. Kini RM, Evans HJ: **The role of enzymatic activity in inhibition of the extrinsic tenase complex by phospholipase A2 isoenzymes from Naja nigricollis venom.** *Toxicon* 1995, **33(12):**1585-1590.
44. Verheij HM, Boffa MC, Rothen C, Bryckaert MC, Verger R, de Haas GH: **Correlation of enzymatic activity and anticoagulant properties of phospholipase A2.** *Eur J Biochem* 1980, **112(1):**25-32.
45. Zhong X, Liu J, Wu X, Zhou Y: **Expression, purification and biochemical characterization of a recombinant phospholipase A2, with anticoagulant activity from Agkistrodon halys Pallas.** *J Nat Toxins* 2001, **10(1):**17-25.
46. Andriao-Escarso SH, Soares AM, Rodrigues VM, Angulo Y, Diaz C, Lomonte B, Gutierrez JM, Giglio JR: **Myotoxic phospholipases A(2) in bothrops snake venoms: effect of chemical modifications on the enzymatic and pharmacological properties of bothropstoxins from Bothrops jararacussu.** *Biochimie* 2000, **82(8):**755-763.
47. Ouyang C, Jy W, Zan YP, Teng CM: **Mechanism of the anticoagulant action of phospholipase A purified from Trimeresurus mucrosquamatus (Formosan habu) snake venom.** *Toxicon* 1981, **19(1):**113-120.
48. Prigent-Dachary J, Boffa MC, Boisseau MR, Dufourcq J: **Snake venom phospholipases A2. A fluorescence study of their binding to phospholipid vesicles correlation with their anticoagulant activities.** *J Biol Chem* 1980, **255(16):**7734-7739.
49. Babu AS, Gowda TV: **Dissociation of enzymatic activity from toxic properties of the most basic phospholipase A2 from Vipera russelli snake venom by guanidination of lysine residues.** *Toxicon* 1994, **32(6):**749-752.
50. Mounier CM, Hackeng TM, Schaeffer F, Faure G, Bon C, Griffin JH: **Inhibition of prothrombinase by human secretory phospholipase A2 involves binding to factor Xa.** *J Biol Chem* 1998, **273(37):**23764-23772.
51. Mounier CM, Luchetta P, Lecut C, Koduri RS, Faure G, Lambeau G, Valentin E, Singer A, Ghomashchi F, Beguin S, Gelb MH, Bon C: **Basic residues of human group IIA phospholipase A2 are important for binding to factor Xa and prothrombinase inhibition comparison with other mammalian secreted phospholipases A2.** *Eur J Biochem* 2000, **267(16):**4960-4969.
52. Carredano E, Westerlund B, Persson B, Saarinen M, Ramaswamy S, Eaker D, Eklund H: **The three-dimensional structures of two toxins from snake venom throw light on the anticoagulant and neurotoxic sites of phospholipase A2.** *Toxicon* 1998, **36(1):**75-92.
53. Singh G, Gourinath S, Sharma S, Para masivam M, Srinivasan A, Singh TP: **Sequence and crystal structure determination of a basic phospholipase A2 from common krait (Bungarus caeruleus) at 2.4 A resolution: identification and characterization of its pharmacological sites.** *J Mol Biol* 2001, **307(4):**1049-1059.
54. Kini RM: **Anticoagulant proteins from snake venoms: structure, function and mechanism.** *Biochem J* 2006, **397(3):**377-387.
55. Faure G, Choumet V, Bouchier C, Camoin L, Guillaume JL, Monegier B, Vuilhorgne M, Bon C: **The origin of the diversity of crotoxin**

isoforms in the venom of Crotalus durissus terrificus. *Eur J Biochem* 1994, **223(1):**161-164.
56. Faure G, Guillaume JL, Camoin L, Saliou B, Bon C: **Multiplicity of acidic subunit isoforms of crotoxin, the phospholipase A2 neurotoxin from Crotalus durissus terrificus venom, results from posttranslational modifications.** *Biochemistry* 1991, **30(32):**8074-8083.
57. Francis B, Bdolah A, Kaiser II: **Amino acid sequences of a heterodimeric neurotoxin from the venom of the false horned viper (Pseudocerastes fieldi).** *Toxicon* 1995, **33(7):**863-874.
58. Ritonja A, Gubensek F: **Ammodytoxin A, a highly lethal phospholipase A2 from Vipera ammodytes ammodytes venom.** *Biochim Biophys Acta* 1985, **828(3):**306-312.
59. Krizaj I, Siigur J, Samel M, Cotic V, Gubensek F: **Isolation, partial characterization and complete amino acid sequence of the toxic phospholipase A2 from the venom of the common viper, Vipera berus berus.** *Biochim Biophys Acta* 1993, **1157(1):**81-85.
60. Nunez V, Arce V, Gutierrez JM, Lomonte B: **Structural and functional characterization of myotoxin I, a Lys49 phospholipase A2 homologue from the venom of the snake Bothrops atrox.** *Toxicon* 2004, **44(1):**91-101.
61. Francis B, Gutierrez JM, Lomonte B, Kaiser II: **Myotoxin II from Bothrops asper (Terciopelo) venom is a lysine-49 phospholipase A2.** *Arch Biochem Biophys* 1991, **284(2):**352-359.
62. Gowda VT, Schmidt J, Middlebrook JL: **Primary sequence determination of the most basic myonecrotic phospholipase A2 from the venom of Vipera russelli.** *Toxicon* 1994, **32(6):**665-673.
63. Pan H, Ou-Yang LL, Yang GZ, Zhou YC, Wu XF: **Cloning of the BPLA(2) Gene from Agkistrodon halys Pallas.** *Sheng Wu Hua Xue Yu Sheng Wu Wu Li Xue Bao (Shanghai)* 1996, **28(6):**579-582.
64. Kondo K, Zhang J, Xu K, Kagamiyama H: **Amino acid sequence of a presynaptic neurotoxin, agkistrodotoxin, from the venom of Agkistrodon halys Pallas.** *J Biochem (Tokyo)* 1989, **105(2):**196-203.
65. Randolph A, Heinrikson RL: **Crotalus atrox phospholipase A2. Amino acid sequence and studies on the function of the NH2-terminal region.** *J Biol Chem* 1982, **257(5):**2155-2161.
66. Kramer RM, Hession C, Johansen B, Hayes G, McGray P, Chow EP, Tizard R, Pepinsky RB: **Structure and properties of a human non-pancreatic phospholipase A2.** *J Biol Chem* 1989, **264(10):**5768-5775.
67. Faure G, Bon C: **Crotoxin, a phospholipase A2 neurotoxin from the South American rattlesnake Crotalus durissus terrificus: purification of several isoforms and comparison of their molecular structure and of their biological activities.** *Biochemistry* 1988, **27(2):**730-738.
68. Faure G, Harvey AL, Thomson E, Saliou B, Radvanyi F, Bon C: **Comparison of crotoxin isoforms reveals that stability of the complex plays a major role in its pharmacological action.** *Eur J Biochem* 1993, **214(2):**491-496.
69. Faure G, Fourier A: **SPR study to characterize the snake venom phospholipases A2 mechanism of action.** In *Toxines et Cancer* Edited by: Goudey-Perrière F, Benoit E, Goyffon M, Marchot P. Paris: Elsevier; 2006 in press.
70. Choumet V, Lafaye P, Mazie JC, Bon C: **A monoclonal antibody directed against the non-toxic subunit of a dimeric phospholipase A2 neurotoxin, crotoxin, neutralizes its toxicity.** *Biol Chem* 1998, **379(7):**899-906.
71. Dorandeu F, Hesters R, Girard F, Four E, Foquin A, Bon C, Lallement G, Faure G: **Inhibition of crotoxin phospholipase A(2) activity by manoalide associated with inactivation of crotoxin toxicity and dissociation of the heterodimeric neurotoxic complex.** *Biochem Pharmacol* 2002, **63(4):**755-761.
72. Tsai CJ, Lin SL, Wolfson HJ, Nussinov R: **Studies of protein-protein interfaces: a statistical analysis of the hydrophobic effect.** *Protein Sci* 1997, **6(1):**53-64.
73. Sobolev V, Sorokine A, Prilusky J, Abola EE, Edelman M: **Automated analysis of interatomic contacts in proteins.** *Bioinformatics* 1999, **15(4):**327-332.
74. Kasturi S, Rudrammaji LM, Gowda TV: **Antibodies to a phospholipase A2 from Vipera russelli selectively neutralize venom neurotoxicity.** *Immunology* 1990, **70(2):**175-180.
75. Zhao K, Zhou Y, Lin Z: **Structure of basic phospholipase A2 from Agkistrodon halys Pallas: implications for its association, hemolytic and anticoagulant activities.** *Toxicon* 2000, **38(7):**901-916.
76. Zhong X, Jiao H, Fan L, Wu X, Zhou Y: **Functionally important residues for the anticoagulant activity of a basic phospholipase A(2) from the Agkistrodon halys pallas.** *Protein Pept Lett* 2002, **9(5):**427-434.
77. Scott DL, Mandel AM, Sigler PB, Honig B: **The electrostatic basis for the interfacial binding of secretory phospholipases A2.** *Biophys J* 1994, **67(2):**493-504.
78. Chattopadhyay A, James HL, Fair DS: **Molecular recognition sites on factor Xa which participate in the prothrombinase complex.** *J Biol Chem* 1992, **267(17):**12323-12329.
79. Rezaie AR: **Identification of basic residues in the heparin-binding exosite of factor Xa critical for heparin and factor Va binding.** *J Biol Chem* 2000, **275(5):**3320-3327.
80. Rudolph AE, Porche-Sorbet R, Miletich JP: **Substitution of asparagine for arginine 347 of recombinant factor Xa markedly reduces factor Va binding.** *Biochemistry* 2000, **39(11):**2861-2867.
81. Rudolph AE, Porche-Sorbet R, Miletich JP: **Definition of a factor Va binding site in factor Xa.** *J Biol Chem* 2001, **276(7):**5123-5128.
82. Rezaie AR, Kittur FS: **The critical role of the 185–189-loop in the factor Xa interaction with Na+ and factor Va in the prothrombinase complex.** *J Biol Chem* 2004, **279(46):**48262-48269.
83. Yegneswaran S, Mesters RM, Griffin JH: **Identification of distinct sequences in human blood coagulation factor Xa and prothrombin essential for substrate and cofactor recognition in the prothrombinase complex.** *J Biol Chem* 2003, **278(35):**33312-33318.
84. Murakami MT, Rios-Steiner J, Weaver SE, Tulinsky A, Geiger JH, Arni RK: **Intermolecular interactions and characterization of the novel factor Xa exosite involved in macromolecular recognition and inhibition: crystal structure of human Gla-domainless factor Xa complexed with the anticoagulant protein NAPc2 from the hematophagous nematode Ancylostoma caninum.** *J Mol Biol* 2007, **366(2):**602-610.
85. Rios-Steiner JL, Murakami MT, Tulinsky A, Arni RK: **Active and Exo-site Inhibition of Human Factor Xa: Structure of des-Gla Factor Xa Inhibited by NAP5, a Potent Nematode Anticoagulant Protein from Ancylostoma caninum.** *J Mol Biol* 2007, **371(3):**774-786.
86. Kasturi S, Gowda TV: **Detection, using antibodies, of pharmacologically active sites, apart from the catalytic site, on venom phospholipase A2.** *Toxicon* 1990, **28(1):**91-99.
87. Prijatelj P, Copic A, Krizaj I, Gubensek F, Pungercar J: **Charge reversal of ammodytoxin A, a phospholipase A2-toxin, does not abolish its neurotoxicity.** *Biochem J* 2000, **352(Pt 2):**251-255.
88. Bdolah A, Kinamon S, Batzri-Izraeli R: **The neurotoxic complex from the venom of Pseudocerastes fieldi. Contribution of the nontoxic subunit.** *Biochem Int* 1985, **11(4):**627-636.
89. Mounier C, Franken PA, Verheij HM, Bon C: **The anticoagulant effect of the human secretory phospholipase A2 on blood plasma and on a cell-free system is due to a phospholipid-independent mechanism of action involving the inhibition of factor Va.** *Eur J Biochem* 1996, **237(3):**778-785.
90. Nazare M, Will DW, Matter H, Schreuder H, Ritter K, Urmann M, Essrich M, Bauer A, Wagner M, Czech J, Lorenz M, Laux V, Wehner V: **Probing the subpockets of factor Xa reveals two binding modes for inhibitors based on a 2-carboxyindole scaffold: a study combining structure-activity relationship and X-ray crystallography.** *J Med Chem* 2005, **48(14):**4511-4525.
91. Lipman DJ, Pearson WR: **Rapid and sensitive protein similarity searches.** *Science* 1985, **227(4693):**1435-1441.
92. Pearson WR, Lipman DJ: **Improved tools for biological sequence comparison.** *Proc Natl Acad Sci U S A* 1988, **85(8):**2444-2448.
93. **Weblogo** [http://weblogo.berkeley.edu/logo.cgi]
94. Crooks GE, Hon G, Chandonia JM, Brenner SE: **WebLogo: a sequence logo generator.** *Genome Res* 2004, **14(6):**1188-1190.
95. Berman HM, Westbrook J, Feng Z, Gilliland G, Bhat TN, Weissig H, Shindyalov IN, Bourne PE: **The Protein Data Bank.** *Nucleic Acids Res* 2000, **28(1):**235-242.
96. Tang L, Zhou YC, Lin ZJ: **Crystal structure of agkistrodotoxin, a phospholipase A2-type presynaptic neurotoxin from agkistrodon halys pallas.** *J Mol Biol* 1998, **282(1):**1-11.
97. Chandra V, Kaur P, Jasti J, Betzel C, Singh TP: **Regulation of catalytic function by molecular association: structure of phospholipase A2 from Daboia russelli pulchella (DPLA2) at 1.9**

A resolution. *Acta Crystallogr D Biol Crystallogr* 2001, **57(Pt 12):**1793-1798.
98. Ward RJ, de Azevedo WF Jr, Arni RK: **At the interface: crystal structures of phospholipases A2.** *Toxicon* 1998, **36(11):**1623-1633.
99. Brunie S, Bolin J, Gewirth D, Sigler PB: **The refined crystal structure of dimeric phospholipase A2 at 2.5 A. Access to a shielded catalytic center.** *J Biol Chem* 1985, **260(17):**9742-9749.
100. Zhao K, Song S, Lin Z, Zhou Y: **Structure of a basic phospholipase A2 from Agkistrodon halys Pallas at 2.13 A resolution.** *Acta Crystallogr D Biol Crystallogr* 1998, **54(Pt 4):**510-521.
101. Schneidman-Duhovny D, Inbar Y, Polak V, Shatsky M, Halperin I, Benyamini H, Barzilai A, Dror O, Haspel N, Nussinov R, Wolfson HJ: **Taking geometry to its edge: fast unbound rigid (and hinge-bent) docking.** *Proteins* 2003, **52(1):**107-112.
102. Canutescu AA, Shelenkov AA, Dunbrack RL Jr: **A graph-theory algorithm for rapid protein side-chain prediction.** *Protein Sci* 2003, **12(9):**2001-2014.
103. **PPI-Pred** [http://www.bioinformatics.leeds.ac.uk/ppi_pred/]
104. **PISA** [http://www.ebi.ac.uk/msd-srv/prot_int/pistart.html]
105. Henrick EKaK: **Detection of Protein Assemblies in Crystals.** *Volume 3695*. Konstanz: Springer Berlin/Heidelberg; 2005.
106. [http://ligin.weizmann.ac.il/space/].
107. Sobolev V, Eyal E, Gerzon S, Potapov V, Babor M, Prilusky J, Edelman M: **SPACE: a suite of tools for protein structure prediction and analysis based on complementarity and environment.** *Nucleic Acids Res* 2005:W39-43.